Development of $L1_0$-ordered FePt with low damping and large perpendicular magnetic anisotropy by engineering the nanostructure

P. D. Bentley,[1, 2, a)] Y. Sasaki,[1, b)] I. Suzuki,[1] S. Isogami,[1] Y. K. Takahashi,[1] and H. Suto[1, c)]
[1)]*National Institute for Materials Science, Tsukuba, Ibaraki 305-0047, Japan*
[2)]*Kansai Institute for Photon Science, National Institutes for Quantum Science and Technology, 8-1-7 Umemidai Kizugawa, Kyoto 619-0215, Japan*

(Dated: 11 December 2024)

THz spintronics is an emergent area of research aimed at bridging the gap between 5th and 6th Generation wireless telecommunications by utilizing new spintronic devices such as magnetic spin torque oscillators as a source of low powered THz emission. The realization of such devices using ferromagnetic metal thin films however requires magnetic materials with both large perpendicular magnetic anisotropy and low Gilbert damping constants. In this letter we report on the development of $L1_0$-ordered FePt with an effective Gilbert damping constant as low as 0.033. Using time-resolved magneto-optical Kerr effect, we characterized the magnetization dynamics of continuous $L1_0$-ordered FePt grown on MgO and $SrTiO_3$ substrates. By changing the substrate on which FePt is grown, the lattice mismatch and subsequent number of misfit dislocations at the interface and $L1_0$-ordering can be controlled. We found that fewer misfits and improved ordering in FePt lead to a reduced Gilbert damping constant due to reduced electron scattering but that FePt grown on $SrTiO_3$ also shows robust perpendicular magnetic anisotropy. Importantly, these results demonstrate the ability to control the damping in FePt and similar materials by changing the number of misfit dislocations at the interface and the smaller damping in FePt opens up the possibility of using this material in spintronic materials in the THz wave range.

In the current realm of big data acquisition and utilization, where data density requirements have escalated to new levels, there have been increasing demands for improved high-speed and-capacity communication network technologies. These requirements drive the advancement of innovative solutions to ensure seamless and efficient data handling in an increasingly connected world. Sixth-generation wireless technology (6G) is the next stage in mobile communications, where the electromagnetic wave frequency range used for 6G partially includes terahertz waves which are those within the frequency range of 100 GHz to 10 THz.[1,2] Therefore, the realization of oscillators and detectors which operate in the THz wave range are an important building block in the future of the Internet of Things.

Recently, using magnetoresistance in ferromagnetic (or ferrimagnetic) metal, insulator, ferromagnetic thin film heterostructures, spin-torque/spin-Hall nano-oscillators have been developed which act as micro to millimeter wave emitters and or detectors.[3–10] To achieve spintronic devices with THz operating frequencies, theoretical studies have mainly focused on using antiferromagnetic materials owing to their antiferromagnetic resonance frequencies in the THz gap.[11–14] However in terms of experimental devices, spintronic emitter and detector devices have been demonstrated primarily using ferromagnetic materials because of their large magnetoresistance effect, large saturation magnetization, and efficient control of their magnetization owing to their high spin injection efficiency and small damping constant α.[15–17] Unfortunately ferromagnetic-based systems have struggled to achieve THz operation so far as these spintronic devices require magnetic materials with effective anisotropy fields above 3.0 T which give rise to the high magnetization precession frequencies needed.

Due to its large magnetoresistance, high spin current injection efficiency,[18] and anomalous spin Hall effect,[19] $L1_0$-ordered FePt is a promising candidate material for various spintronic applications. Its huge perpendicular magnetic anisotropy (PMA) energy above 4.5 MJ m^{-3} is already being used in magnetic recording media applications such as hard disk drives, and its anisotropy field is high enough in principle for THz wave use.[20–22]

Since the magnetization dynamics of $L1_0$-FePt are in the THz wave range, conventional electrical measurements are challenging therefore necessitating the use of all-optical methods such as time-resolved magneto-optical Kerr effect (TRMOKE) measurements with ultrashort laser pulses to measure the damping constant of this material.[23,24] Consequently, there are very few studies which report on the Gilbert damping constant in $L1_0$-FePt, and there is no research specifically focused on reducing the damping of this material. Although previous measurements of the damping constant of $L1_0$-FePt have reported a relatively large value ranging from $0.05 - 0.26$,[25–28] overcoming this drawback and reducing the damping in $L1_0$-FePt could lead to the realization of practical ferromagnetic metal thin films for THz spintronic devices, thus making this material a desirable candidate for these applications.

In this study, we aimed to reduce the damping constant of $L1_0$-FePt by controlling the fine nanostructure and reducing the number of misfit dislocations observed using transmission electron microscopy (TEM). Theoretically, the damping constant of $L1_0$-FePt is primarily influenced by electron impurity scattering, and both theoretically and experimentally, it is expected to vary with changes in the electron impurity scattering rate, however this is difficult to control or modify.[29,30] Through fine structural evaluation and terahertz magnetiza-

[a)]Electronic mail: bentley.phillip@qst.go.jp
[b)]Electronic mail: sasaki.yuta@nims.go.jp
[c)]Electronic mail: suto.hirofumi@nims.go.jp

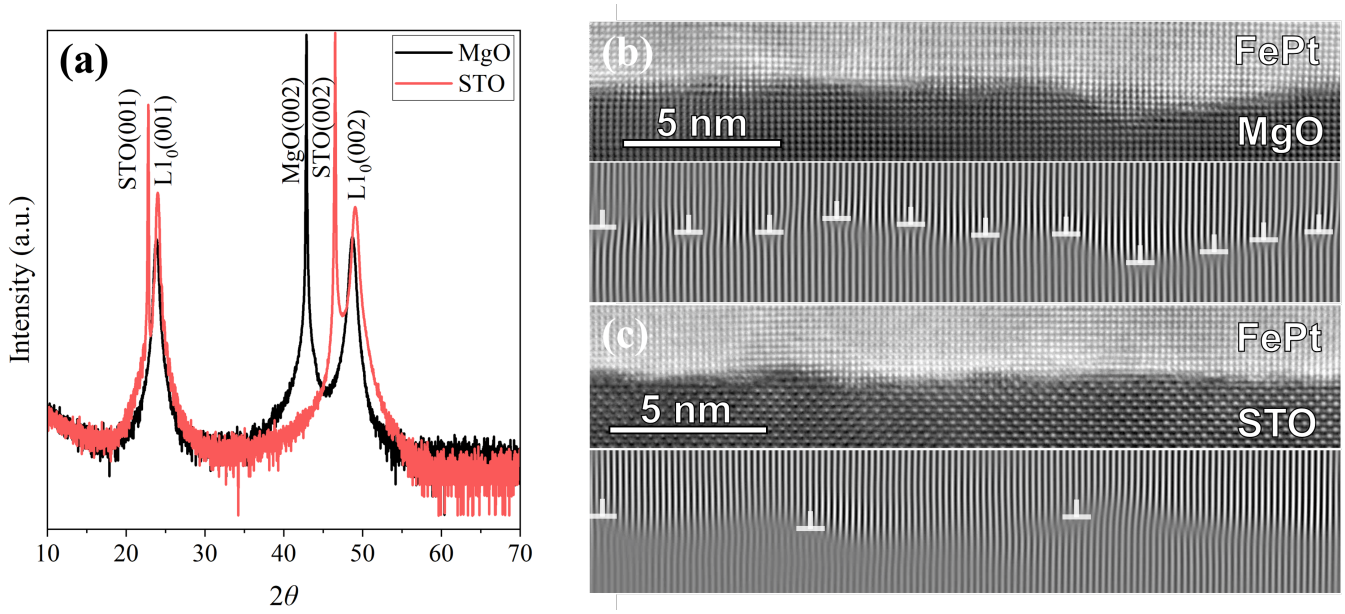

FIG. 1. (a) XRD profiles of 30 nm continuous FePt thin films grown on MgO and STO substrates showing the presence of $L1_0$-ordered FePt, (b) and (c) cross-sectional STEM images of FePt/MgO and FePt/STO, respectively, where the change in contrast represents the difference between the substrate and the FePt thin film, the white markers highlight misfit dislocations, and the lower subfigure of (b) and (c) are inverse Fourier filtered transformation images of the STEM images shown in the upper subfigure.

tion dynamics analysis using light, we successfully reduced the damping constant from the previously reported value of 0.05[28] to 0.033 by controlling the number of misfit dislocations. These results suggest that reducing the damping constant through fine structural control of the nanostructure, enable the application of materials such as $L1_0$-FePt which have not been extensively explored for spintronic devices beyond magnetic recording, for applications in the THz wave range.

Continuous thin films of FePt were deposited on single-crystalline MgO(001) and $SrTiO_3$(001) (STO) substrates at a deposition temperature of 400°C via magnetron sputtering in an ultrahigh vacuum chamber with a base pressure of 8×10^{-7} Pa and an Ar pressure of 0.5 Pa during sputtering. Both substrates were annealed at 650 °C for 1 hour before deposition of the FePt film to remove contamination at the surface of the substrate. A $Fe_{51}Pt_{49}$ target was used and compositional analysis of each of the samples showed a stoichiometric $Fe_{50}Pt_{50}$ composition. Structural properties of these thin films were evaluated using X-ray diffraction (XRD) using Cu $K\alpha$ X-rays. Cross-sectional scanning transmission electron microscopy (STEM) measurements were carried out using a SpectraUltra S/TEM (Thermo Fisher Scientific) and the STEM samples were fabricated by focused ion beam (FIB) with a scanning electron microscopy (SEM) dual-beam system Helios5UX (Thermo Fisher Scientific). Magnetic properties of the FePt thin films were evaluated using two superconducting quantum interference device (SQUID) systems, one measured up to 7 T at room temperature and the other up to 14 T to evaluate the anisotropy field and PMA of these thin films. TRMOKE was performed using a Quantum Design Opticool system with laser pump and probe beam diameters 120 μm and 80 μm, and laser fluences of 1.33 mJ cm^{-2} and 0.99 mJ cm^{-2}, respectively, and fixed magnetic field angles of 80° and 45° to measure closer to and further away from the easy magnetization axis of the sample. The magnetic field angle is measured is relative to the normal of the film plane and the optical setup used in these experiments is described in greater detail elsewhere.[28]

Figure 1(a) shows XRD profiles of the FePt/MgO and the FePt/STO sample where $L1_0$ order is observed in both FePt thin films.[31,32] The (001) and (002) peak positions for the FePt/STO sample are shifted to slightly higher angles relative to the FePt/MgO sample indicating a smaller out-of-plane (OOP) lattice constant (c), which is a result of the smaller in-plane (IP) lattice constant (a) of STO (3.91 Å) relative to MgO (4.20 Å).[33] Similar to previous reports,[34] the c for FePt/MgO and FePt/STO were found to be 3.73 Å and 3.71 Å, respectively. Using STEM, the in-plane lattice constant for both samples was measured to be 3.85 Å and therefore the c/a ratio for the FePt/MgO and FePt/STO sample are ≈ 0.969 and ≈ 0.964, whilst mismatch between FePt and the substrate are 8.33% and 1.41%, respectively. Using the peak intensities of the (001) superlattice peak and the (002) fundamental peak and the formula described in,[35–37] the order parameter, defined as $S_{L10} = \sqrt{I^{exp}_{100}/I^{exp}_{200}}/\sqrt{I^{calc}_{100}/I^{calc}_{200}}$ which is $\approx 0.85\sqrt{I^{exp}_{100}/I^{exp}_{200}}$ where I is the experimental (exp) and calculated (calc) intensities of the (100) and (200) reflections, for these two samples were calculated to be ≈ 0.70 for the FePt/MgO sample and ≈ 0.82 for the FePt/STO sample. High-resolution cross-sectional STEM seen in Figure 1(b) and 1(c) show sharp interfaces for both FePt samples but a smaller number of misfit dislocations for the FePt/STO sample.

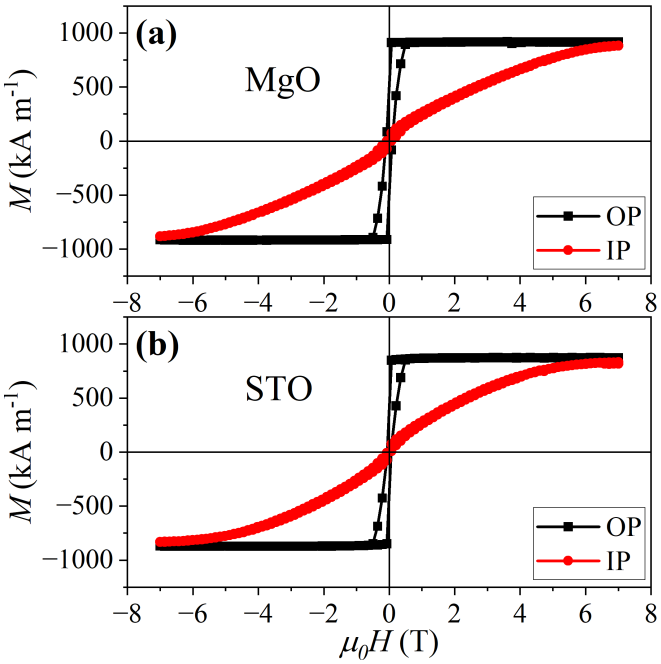

FIG. 2. In-plane (IP) and out-of-plane (OP) magnetization curves measured at room temperature for 30 nm continuous FePt thin films grown on (a) MgO and (b) STO.

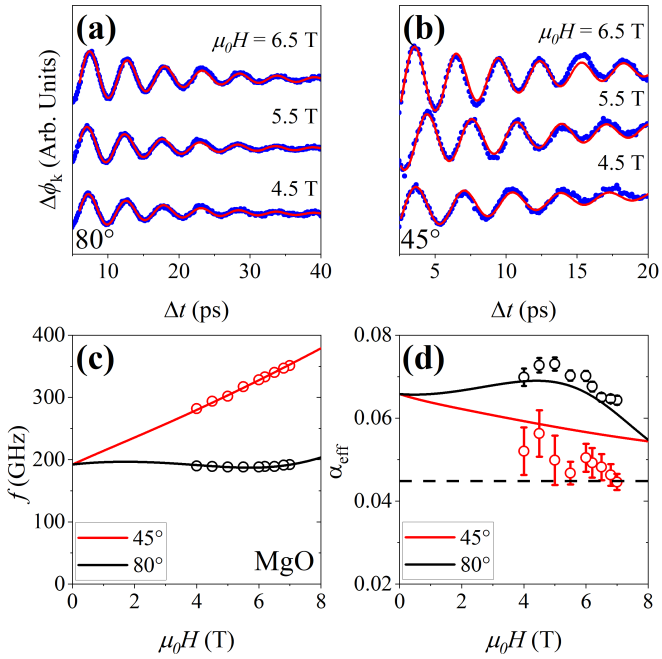

FIG. 3. TRMOKE spectra at different magnetic field strengths for the continuous 30 nm FePt/MgO film at magnetic field angles of (a) 80° and (b) 45°, respectively. The solid red curves represent the fitting of the blue dot raw data. Calculated (c) precession frequency f and (d) effective damping constant α_{eff} as a function of the applied magnetic field at these different magnetic field angles. Solid curves here represent the fitting using the second-order Kittel functions. The dashed line highlights the minimum α_{eff} which for the FePt/MgO sample is around 0.045.

Figure 2(a) and 2(b) show the magnetization curves for the FePt/MgO and FePt/STO sample, respectively. The OP magnetization curve for both samples exhibit a similar shape and are consistent with continuous FePt thin films prepared at these temperatures.[33,38] The anisotropy field of the FePt/MgO and the FePt/STO sample are found to be $\mu_0 H_{\text{k}} = 6.80$ T and $\mu_0 H_{\text{k}} = 5.57$ T and by calculating the area underneath the first quadrant of the magnetization curve of both samples, the PMA was determined to be ≈ 2.26 MJ m^{-3} and ≈ 1.79 MJ m^{-3}, respectively. According to Sakuma *et al.*, the weaker PMA in the FePt/STO sample can be explained to be a result of a smaller lattice mismatch between the FePt and the substrate.[39]

Typical TRMOKE signals obtained for the FePt/MgO sample measured at magnetic field angles $\theta_{\text{H}} = 80°$ and 45° can be seen in Figure 3(a) and 3(b), respectively. Damped oscillation signals relating to magnetization precessional motion were clearly observed for both magnetic field angles. To fit the TRMOKE spectra at different magnetic field strengths and θ_{H} of both samples as seen in Figure 3(a) and 3(b) for the FePt/MgO sample, and Figure 4(a) and 4(b) for the FePt/STO sample, the following function was used which is a least squares method accounting for the exponential recovery of the background signal:

$$\Delta\phi_k = A_0 + A_1 e^{-\nu\Delta t} + B_0 e^{-\Delta t/\tau} \sin(2\pi f \Delta t + \phi) \qquad (1)$$

where the first and second terms represent the magnetization recovery process and the third term represents the magnetization precession in the damped oscillation signal.[28,40] In this equation, B_0 is the precession amplitude, τ lifetime, f frequency, and ϕ the initial phase. The effective damping α_{eff} was then calculated using the equation $\alpha_{\text{eff}} = 1/2\pi f\tau$. TRMOKE spectra between 4 T and 7 T were fitted and the precession frequency and effective damping for these different magnetic field strengths plotted as seen in Figure 3(c) and 3(d), respectively.

To fit the parameters extracted from the raw spectra, second-order equations derived from the Landau-Lifshitz-Gilbert (LLG) equation $f = (\gamma\mu_0/2\pi)\sqrt{H_1 H_2}$, where $\gamma = g\mu_{\text{B}}/\hbar$ is the gyromagnetic ratio. g, μ_{B}, and $\hbar$ are the spectroscopic splitting g-factor, the Bohr magneton, and the reduced Planck's constant, respectively, were used. $H_1 = H\cos(\theta_{\text{H}} - \theta_{\text{M}}) + H_{\text{k}}^{\text{eff}}\cos^2(\theta_{\text{M}}) - H_{\text{k2}}\cos^4(\theta_{\text{M}})$ and $H_2 = H\cos(\theta_{\text{H}} - \theta_{\text{M}}) + H_{\text{k}}^{\text{eff}}\cos(2\theta_{\text{M}}) - \frac{1}{2}H_{\text{k2}}(\cos(2\theta_{\text{M}}) + \cos(4\theta_{\text{M}}))$, where H, $H_{\text{k}}^{\text{eff}}$, H_{k2} are the external magnetic field, effective perpendicular magnetic anisotropy (PMA) field, and second order PMA field, respectively.[41,42] Simultaneously, the magnetization angle θ_{M} was calculated using the relation $2H\sin(\theta_{\text{H}} - \theta_{\text{M}}) - H_{\text{k}}^{\text{eff}}\sin(2\theta_{\text{M}}) + H_{\text{k2}}\cos^2(\theta_{\text{M}})\sin(2\theta_{\text{M}}) = 0$.[28] The life time was calculated using the equation $1/\tau = \alpha\gamma(H_1 + H_2)/2\pi$, where α is the intrinsic magnetic damping constant. As a small laser fluence was used in all measurements, we observed no temperature variance in any of our measurements and therefore the Landau-Lifshitz-Bloch equation was not used in our analysis.[28]

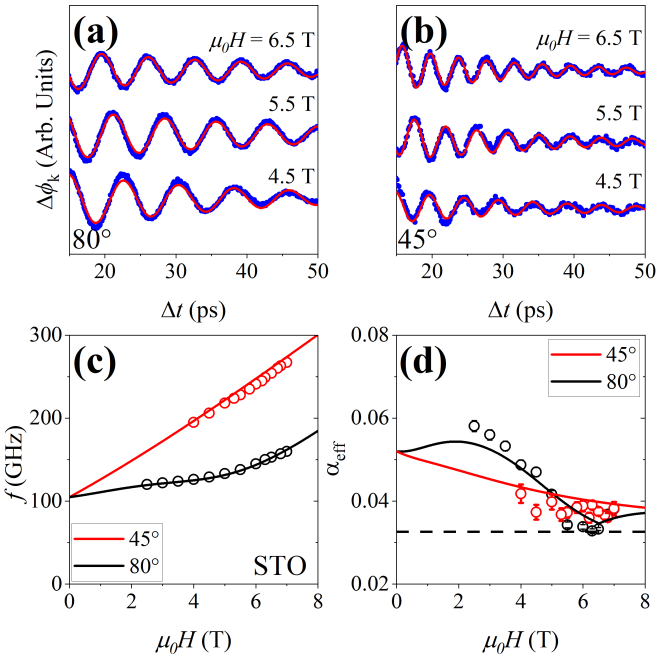

FIG. 4. TRMOKE spectra at different magnetic fields for the continuous 30 nm FePt/STO film at magnetic field angles of (a) 80° and (b) 45°, respectively. Calculated (c) f and (d) α_{eff} as a function of the applied magnetic field at these different magnetic field angles. The minimum α_{eff} for the FePt/STO sample is around 0.033.

The solid lines seen in Figure 3(c) represent the fitting of the precession frequency using the above equations for the MgO sample at both angles, whilst the solid curves seen in Figure 3(d) were calculated by approximating the magnitude of the PMA distribution ΔH_k^{eff} as:

$$1/\tau^{Hk} = \pi \left| \frac{df}{dH_k^{eff}} \right| \Delta H_k^{eff} \quad (2)$$

where the final ΔH_k^{eff} for the FePt/MgO and FePt/STO sample were 250 mT and 136 mT, respectively. The precession frequency monotonically increases with magnetic field for both magnetic field angles 80° and 45°[28,43] whilst the effective damping constant was found to increase with decreasing magnetic field strength showing a minimum value at a magnetic field strength of 7 T (upper limit of the equipment used here) of ≈ 0.045 as highlighted by the dashed line in Figure 3(d); this was similarly performed for the FePt/STO sample as seen in Figure 4(d). The relationship between α_{eff} and μ_0H is a result of the dephasing effect and fewer magnetic domains at higher applied magnetic fields since at 7 T, the FePt thin film approaches a single domain state and there is consequently less dephasing of the spins (spins precessing at different phases) between the few remaining magnetic domains.[44] From the fitting of the magnetization dynamics parameters, the $\mu_0H_k^{eff}$, μ_0H_{k2}, and g-factor of the FePt/MgO sample were determined to be 6.34 ± 0.57 T, 0.33 ± 0.04 T, and 2.29 ± 0.02, respectively.

As seen in Figure 4(c) an 4(d), TRMOKE at magnetic field angles 80° to 45° was also performed for the FePt/STO sample. Similar to the FePt/MgO sample, the precession frequency increases monotonically with magnetic field whilst the damping constant decreases. The $\mu_0H_k^{eff}$, μ_0H_{k2}, and g-factor for FePt/STO were determined to be 4.72 ± 0.01 T, 1.14 ± 0.001 T, and 2.09 ± 0.01, respectively. The smaller $\mu_0H_k^{eff}$ in the FePt/STO continuous thin film is consistent with a smaller PMA observed in this sample with respect to that seen in FePt/MgO. Comparing the calculated g-factor of both samples, the smaller constant observed in the FePt/STO sample is a result of differences in $L1_0$ order where increased disorder in FePt has been found to lead to a monotonic increase in the g-factor.[44] Since the $L1_0$ order parameter in FePt/STO is greater than that in the MgO sample there is therefore less disorder in this system and consequently it has a smaller g-factor.

As seen in Figure 3(d) and Figure 4(d), the effective damping constant α_{eff} at different magnetic field strength evaluated from the TRMOKE data at $\theta_H = 80°$, is well reproduced by considering the magnitude of the PMA distribution using Equation 2. From this fitting, the intrinsic damping constant for the FePt/MgO sample and the FePt/STO sample were calculated to be $\alpha = 0.045$ and 0.033, respectively. Since α_{eff} corresponds to the upper-bound value of α, the minimum effective damping constant is identical to or larger than the intrinsic damping constant. Therefore, as highlighted by the dashed line in both Figure 3(d) and Figure 4(d), we have also plotted the minimum value of the effective damping constant as a function of both θ_H for both samples which is found to be the same as the intrinsic damping constant in both cases.

From a recent theoretical study, it has been reported that the damping constant in $L1_0$-ordered FePt is largely influenced by electron impurity scattering[29] instead of thermal lattice expansion or c/a modification.[45–47] From our TEM measurements, we observed a far higher number of misfit dislocations near the interface for the FePt/MgO sample than for the FePt/STO sample. These misfit dislocations can be considered as impurity scattering centers which increase electron impurity scattering in $L1_0$-ordered FePt and therefore modify α resulting in the observation of a lower magnetic damping constant for the FePt/STO sample since it has fewer misfit dislocations than the FePt/MgO sample. It should be noted that previously it has been suggested that a self-assembled network of misfit dislocation leads to an increase in extrinsic effects such as two-magnon scattering which modify the damping in magnetic metal thin films.[48,49] However, since the measurements presented here were carried out at high magnetic fields, these effects can be ignored.[42] Another possible explanation as why the damping constant is smaller in the FePt/STO sample is due to its smaller PMA since both PMA and damping are related to the spin-orbit interaction. However, we have managed to grow FePt on STO which has a similar frequency and PMA to that grown on MgO. Whilst the damping constant in this sample is not as small as 0.033, it still shows a smaller damping constant than the MgO substrate sample (see the Supplemental Material 50) Importantly, our results demonstrate that by limiting the amount of misfit dislocations and other nanostructural factors that may occur during the manufacturing process

of magnetic materials such as $L1_0$-ordered FePt, we can control their damping opening up the possibility of using this material and similar materials for spintronic applications in the THz wave range. In particular, α as low as 0.01 has been reported theoretically in $L1_0$-FePt,[51] however these calculations as well as other calculations which have focused on the damping in magnetic materials, did not incorporate misfit dislocations. Therefore, given the results presented here even smaller damping in $L1_0$-FePt may be achievable experimentally.

In summary, we have demonstrated that the damping constant in $L1_0$-ordered FePt can be modified by controlling the number of misfit dislocations at the interface of the material. By changing the substrate which FePt is grown on from MgO to STO, the lattice mismatch and subsequent number of misfit dislocations are reduced. We find that the FePt/STO sample shows improved $L1_0$ order compared to the FePt/MgO sample and only a small difference in the PMA between both samples. TRMOKE of the FePt/STO sample show an α_{eff} as small as 0.033, smaller than that of the FePt/MgO sample, 0.045, as a result of smaller number of misfit dislocations at the interface which subsequently modify the number of inter-band and intra-band electron transitions and the electron scattering rate in FePt. Importantly, we show that the damping in FePt can be reduced which thus opens up the possibility of using this material and similar materials for spintronic applications in the THz wave range.

We acknowledge Yukie Mori for the preparation of the samples for cross-sectional TEM measurements. We also acknowledge support from the Japan Science and Technology Agency (JST) Core Research for Evolutional Science and Technology (CREST) (Grant No. JPMJC22C3), the Ministry of Education, Culture, Sports, Science and Technology (MEXT) Leading Initiative for Excellent Young Researchers (Grant No. JPMXS0320230032), and the Japan Society for the Promotion of Science (JSPS) KAKENHI (Grant Nos. JP21K14218 and JP18H03787). A part of this work was supported by the Electron Microscopy Unit, National Institute for Materials Science (NIMS).

AUTHOR DECLARATIONS

Conflict of Interest

The authors have no conflicts to disclose.

Author Contributions

Phillip David Bentley: Conceptulization (supporting); Data curation (equal); Formal analysis (equal); Investigation (equal); Methodology (equal); Project administration (supporting); Validation (equal); Visualization (lead); Writing – original draft (lead); Writing – review & editing (equal). **Yuta Sasaki**: Conceptulization (lead); Data curation (equal); Formal analysis (equal); Funding acquisition (equal); Investigation (equal); Methodology (equal); Project administration (lead); Supervision (lead); Validation (equal); Visualization (supporting); Writing – original draft (supporting); Writing – review & editing (equal). **Ippei Suzuki**: Resources (lead). **Shinji Isogami**: Validation (supporting). **Yukiko Takahashi**: Data curation (equal); Funding acquisition (equal); Investigation (equal); Project Administration (supporting); Supervision (lead); Validation (supporting); Writing – original draft (supporting); Writing – review & editing (equal). **Hirofumi Suto**: Project Administration (supporting); Supervision (lead); Validation (supporting); Writing – original draft (supporting); Writing – review & editing (equal).

DATA AVAILABILITY

The data that support the findings of this study are available from the corresponding author upon reasonable request.

[1] C.-X. Wang, X. You, X. Gao, X. Zhu, Z. Li, C. Zhang, H. Wang, Y. Huang, Y. Chen, H. Haas, J. S. Thompson, E. G. Larsson, M. D. Renzo, W. Tong, P. Zhu, X. Shen, H. V. Poor, and L. Hanzo, IEEE Commun. Surv. Tutor. **25**, 905 (2023).
[2] Z. Zhang, Y. Xiao, Z. Ma, M. Xiao, Z. Ding, X. Lei, G. K. Karagiannidis, and P. Fan, IEEE Veh. Technol. Mag. **14**, 28 (2019).
[3] S. I. Kiselev, J. C. Sankey, I. N. Krivorotov, N. C. Emley, R. J. Schoelkopf, R. A. Buhrman, and D. C. Ralph, Nature **425**, 380 (2003).
[4] S. Miwa, S. Ishibashi, H. Tomita, T. Nozaki, E. Tamura, K. Ando, N. Mizuochi, T. Saruya, H. Kubota, K. Yakushiji, T. Taniguchi, H. Imamura, A. Fukushima, S. Yuasa, and Y. Suzuki, Nat. Mater. **13**, 50 (2014).
[5] H. Ren, X. Y. Zheng, S. Channa, G. Wu, D. A. O'Mahoney, Y. Suzuki, and A. D. Kent, Nat. Commun. **14**, 1406 (2023).
[6] Y. Kurokawa, K. Yamada, T. Taniguchi, S. Horiike, T. Tanaka, and H. Yuasa, Sci. Rep. **12**, 10849 (2022).
[7] I. Volvach, A. Kent, E. Fullerton, and V. Lomakin, Phys. Rev. Appl. **18**, 024071 (2022).
[8] S. Tsunegi, T. Taniguchi, K. Nakajima, S. Miwa, K. Yakushiji, A. Fukushima, S. Yuasa, and H. Kubota, Appl. Phys. Lett. **114**, 164101 (2019).
[9] H. Suto, H. Sepehri-Amin, N. Asam, W. Zhou, A. Bolyachkin, M. Takagishi, N. Narita, S. Tamaru, T. Nakatani, and Y. Sakuraba, Appl. Phys. Express **14**, 053001 (2021).
[10] Y. Nakagawa, M. Takagishi, N. Narita, T. Nagasawa, G. Koizumi, W. Chen, S. Kawasaki, T. Roppongi, A. Takeo, and T. Maeda, Appl. Phys. Lett. **122**, 042403 (2023).
[11] R. Cheng, D. Xiao, and A. Brataas, Phys. Rev. Lett. **116**, 207603 (2016).
[12] R. Ovcharov, E. Galkina, B. Ivanov, and R. Khymyn, Phys. Rev. Appl. **18**, 024047 (2022).
[13] W. Wu, C. Yaw Ameyaw, M. F. Doty, and M. B. Jungfleisch, J. Appl. Phys. **130**, 091101 (2021).
[14] A. Hirohata, K. Yamada, Y. Nakatani, I.-L. Prejbeanu, B. Diény, P. Pirro, and B. Hillebrands, J. Magn. Magn. Mater. **509**, 166711 (2020).
[15] J. Torrejon, M. Riou, F. A. Araujo, S. Tsunegi, G. Khalsa, D. Querlioz, P. Bortolotti, V. Cros, K. Yakushiji, A. Fukushima, H. Kubota, S. Yuasa, M. D. Stiles, and J. Grollier, Nature **547**, 428 (2017).
[16] J. Walowski and M. Münzenberg, J. Appl. Phys. **120**, 140901 (2016).
[17] H. Suto, T. Nagasawa, K. Kudo, K. Mizushima, and R. Sato, Nanotechnology **25**, 245501 (2014).
[18] K. Dong, C. Sun, L. Zhu, Y. Jiao, Y. Tao, X. Hu, R. Li, S. Zhang, Z. Guo, S. Luo, X. Yang, S. Li, and L. You, Eng. J. **12**, 55 (2022).
[19] T. Seki, S. Iihama, T. Taniguchi, and K. Takanashi, Phys. Rev. B **100**, 144427 (2019).
[20] N. Kulesh, A. Bolyachkin, I. Suzuki, Y. Takahashi, H. Sepehri-Amin, and K. Hono, Acta Mater. **255**, 119039 (2023).

[21] N. T. Binh, S. Ruta, O. Hovorka, R. F. L. Evans, and R. W. Chantrell, Phys. Rev. B **106**, 054421 (2022).
[22] J. Waters, D. Kramer, T. Sluckin, and O. Hovorka, Phys. Rev. Appl. **11**, 024028 (2019).
[23] A. Barman, S. Wang, O. Hellwig, A. Berger, E. E. Fullerton, and H. Schmidt, J. Appl. Phys. **101**, 09D102 (2007).
[24] H. J. Mohamad, L. R. Shelford, M. Aziz, U. A. S. Al-Jarah, R. Al-Saigh, R. A. J. Valkass, S. Marmion, B. J. Hickey, and R. J. Hicken, Phys. Rev. B **96**, 134431 (2017).
[25] J.-W. Kim, H.-S. Song, J.-W. Jeong, K.-D. Lee, J.-W. Sohn, T. Shima, and S.-C. Shin, Appl. Phys. Lett. **98**, 092509 (2011).
[26] K.-D. Lee, H.-S. Song, J.-W. Kim, H. S. Ko, J.-W. Sohn, B.-G. Park, and S.-C. Shin, Appl. Phys. Express **7**, 113004 (2014).
[27] J. Becker, O. Mosendz, D. Weller, A. Kirilyuk, J. C. Maan, P. C. M. Christianen, T. Rasing, and A. Kimel, Appl. Phys. Lett. **104**, 152412 (2014).
[28] Y. Sasaki, I. Suzuki, R. Mandal, S. Kasai, and Y. K. Takahashi, ACS Appl. Nano Mater. **6**, 5901 (2023).
[29] I. Kurniawan, Y. Miura, G. Xing, T. Tadano, and K. Hono, Phys. Rev. B **108**, 094426 (2023).
[30] T. Seki, Y. Hasegawa, S. Mitani, S. Takahashi, H. Imamura, S. Maekawa, J. Nitta, and K. Takanashi, Nat. Mater. **7**, 125 (2008).
[31] A. Cebollada, D. Weller, J. Sticht, G. R. Harp, R. F. C. Farrow, R. F. Marks, R. Savoy, and J. C. Scott, Phys. Rev. B **50**, 3419 (1994).
[32] E. Yang, D. E. Laughlin, and J.-G. Zhu, IEEE Trans. Magn. **48**, 7 (2012).
[33] I. Suzuki, S. Kubo, H. Sepehri-Amin, and Y. K. Takahashi, ACS Appl. Mater. Interfaces **13**, 16620 (2021).
[34] A. Hotta, T. Ono, M. Hatayama, K. Tsumura, N. Kikuchi, S. Okamoto, O. Kitakami, and T. Shimatsu, J. Appl. Phys. **115**, 17B712 (2014).
[35] J. Wang, H. Sepehri-Amin, H. Tajiri, T. Nakamura, K. Masuda, Y. Takahashi, T. Ina, T. Uruga, I. Suzuki, Y. Miura, and K. Hono, Acta Mater. **166**, 413 (2019).
[36] I. Suzuki, J. Wang, Y. K. Takahashi, and K. Hono, J. Magn. Magn. Mater. **500**, 166418 (2020).
[37] Y. Dai, Y. W. Zhao, L. Ma, M. Tang, X. P. Qiu, Y. Liu, Z. Yuan, and S. M. Zhou, Phys. Rev. Lett. **128**, 247202 (2022).
[38] Y. Takahashi, K. Hono, T. Shima, and K. Takanashi, J. Magn. Magn. Mater. **267**, 248 (2003).
[39] A. Sakuma, J. Phys. Soc. Jpn. **63**, 3053 (1994).
[40] Y. Liu, L. R. Shelford, V. V. Kruglyak, R. J. Hicken, Y. Sakuraba, M. Oogane, and Y. Ando, Phys. Rev. B **81**, 094402 (2010).
[41] A. Okada, S. Kanai, M. Yamanouchi, S. Ikeda, F. Matsukura, and H. Ohno, Appl. Phys. Lett. **105**, 052415 (2014).
[42] S. Iihama, A. Sakuma, H. Naganuma, M. Oogane, S. Mizukami, and Y. Ando, Phys. Rev. B **94**, 174425 (2016).
[43] S. Mizukami, S. Iihama, N. Inami, T. Hiratsuka, G. Kim, H. Naganuma, M. Oogane, and Y. Ando, Appl. Phys. Lett. **98**, 052501 (2011).
[44] X. Ma, L. Ma, P. He, H. B. Zhao, S. M. Zhou, and G. Lüpke, Phys. Rev. B **91**, 014438 (2015).
[45] A. von Reppert, L. Willig, J.-E. Pudell, S. P. Zeuschner, G. Sellge, F. Ganss, O. Hellwig, J. A. Arregi, V. Uhlíř, A. Crut, and M. Bargheer, Sci. Adv. **6**, eaba1142 (2020).
[46] Y. Sasaki, R. Hiramatsu, Y. Kota, T. Kubota, Y. Sonobe, A. Sakuma, K. Takanashi, S. Kasai, and Y. K. Takahashi, Small **18**, 2200378 (2022).
[47] R. Mandal, J. W. Jung, K. Masuda, Y. K. Takahashi, Y. Sakuraba, S. Kasai, Y. Miura, T. Ohkubo, and K. Hono, Appl. Phys. Lett. **113**, 232406 (2018).
[48] G. Woltersdorf, B. Heinrich, J. Woltersdorf, and R. Scholz, J. Appl. Phys. **95**, 7007 (2004).
[49] B. Kooi, H. Groen, and J. De Hosson, Acta Mater. **46**, 111 (1998).
[50] See Supplemental Material at `URL_will_be_inserted_by_publisher` (2024) for a comparison of FePt grown on MgO and STO with similar PMA.
[51] R. Hiramatsu, D. Miura, and A. Sakuma, Appl. Phys. Express **15**, 013003 (2021).